Hemoprotein Models Based on a Covalent Helix–Heme–Helix Sandwich: 1. Design, Synthesis, and Characterization

Flavia Nastri, Angela Lombardi, Giancarlo Morelli, Ornella Maglio, Gabriella D'Auria, Carlo Pedone, and Vincenzo Pavone*

Abstract: In this paper we describe the design, synthesis, and spectroscopic characterization of a covalent helix–heme–helix sandwich named Fe^{III} *mimochrome* I. It contains deuterohemin bound through both propionyl groups to two identical *N*- and *C*-terminal protected nonapeptides as α-helical scaffolds. Each peptide moiety bears a His residue in the central position, which acts as axial ligand to the metal ion. The newly developed synthetic strategy is based on a combination of solution and solid-phase methodologies. It represents a powerful method for obtaining a large variety of analogues containing two symmetric or unsymmetric peptide chains covalently bound to the deuteroporphyrin ring. UV/Visible spectroscopic characterization in buffered 2,2,2-trifluoroethanol/water solution proves low-spin bis(histidine) iron(III) coordination; circular dichroism (CD) measurements show an α-helical conformation for the peptide moieties. Thus, all the data are in agreement with the designed hypothetical model regarding both the iron(III) coordination and the peptide chain structural organization.

Keywords
helical structures · heme proteins · iron · peptides · synthesis design

Introduction

Synthetic metalloporphyrins are versatile molecules, able to play a key role in a great variety of chemical and physical processes: oxidation reactions,[1] electron transfer,[2] dioxygen transport and storage.[3] The wide range of metalloporphyrin-associated properties can be modulated by a) the chemical structure of the tetrapyrrole ring, here including the substituents on the *meso* or on the β-pyrrole positions, b) the oxidation states and redox potential of the encapsulated metal ion, and c) the presence of different axial ligands. All these factors directly affect the fine structures of metalloporphyrin and consequently determine their spectroscopic, electrochemical, nuclear magnetic, and electron paramagnetic properties.[4]

In natural systems, iron(III) protoporphyrin IX is the common prosthetic group of many hemoproteins. Their different biological functions seem directly related to different donor properties of the axial ligands, to the three-dimensional structure, and to the amino acid composition of the peptide chain surrounding the heme active site.[5] Replacement of the fifth imidazole axial ligand in hemoglobin and myoglobin with thiolate in cytochrome P-450 dependent monooxygenases plays a part in switching the hemoprotein function from reversible dioxygen binding to dioxygen activation. In peroxidases and catalases involved in hydrogen peroxide activation, the fifth axial ligands are generally a histidine and a tyrosine residue, respectively. Finally, cytochromes *c* play a key role in electron transfer, and they are characterized by a histidine/methionine axial ligand combination and particularly by the covalent linkage between the two cysteine residues at positions 7 and 12 of the heme; cytochromes *b*, which also participate in electron transfer, are instead characterized by bis(histidine) axial coordination with an iron ion in the low-spin state.

A finer tuning of hemoprotein properties is accomplished by the polypeptide chain. In fact, iron ion redox potential seems to be modulated by the local environment surrounding the heme.[6] For instance, a large number of positively charged residues around the heme in hemoglobin and in myoglobin may favor a low oxidation state for the iron, making it ready to bind dioxygen. Similarly, the progressive change in the polarity of the surrounding peptide environment from a negative charge distribution in cytochromes *b* to a positive one in cytochromes *c* determines a gradual increase in the Fe^{III}/Fe^{II} redox potential. The resulting stabilization of Fe^{II} and Fe^{III} states enables cytochromes to mediate electron transfer.

To better clarify the many structural and functional aspects of hemoproteins, many efforts have been devoted in the past decades to the design, synthesis, and characterization of a large variety of hemoprotein model compounds.[1–3] They were also developed in order to obtain new, low-molecular-weight com-

[*] Prof. V. Pavone, Dr. F. Nastri, Dr. A. Lombardi, Prof. G. Morelli, Dr. O. Maglio, Dr. G. D'Auria, Prof. C. Pedone
Centro Interdipartimentale di Ricerca sui Peptidi Bioattivi e Centro di studio di Biocristallografia CNR
Via Mezzocannone 4, I-80134 Napoli (Italy)
Fax: Int. code +(81)552-7771
e-mail: pavone@chemna.dichi.unina.it

0947-6539/97/0303-0340 $ 15.00+.25/0

pounds capable of mimicking biological systems and of performing specific chemical reactions. A large number of models of the oxygen-binding proteins hemoglobin and myoglobin[3] have been developed. Carbon monoxide–iron(II) coordination and reversible oxygen binding is made possible by simple iron porphyrin complexes containing bulky and properly designed substituents that prevent irreversible oxidation of the iron.[7] The development of synthetic catalysts that could act as models for cytochromes P-450 has also attracted the interest of many scientists, and metalloporphyrin-based homogeneous[1] or supported catalysts[8] have been synthesized. These simple molecules are able to reproduce the main reaction of the natural enzyme and they are routinely employed in catalysis. However, they partly fail in reproducing the efficient regioselectivity and stereoselectivity of natural hemoproteins since they lack the protein environment necessary for substrate recognition.

In order better to understand the role of the peptide chain composition and folding in the control of the physicochemical properties of hemoproteins, a great deal of attention has also been devoted to the design of peptide-based hemoprotein model compounds. This class of models represents a powerful tool for structure–activity relationship studies, which may help to identify the minimum requirements for defined functions. Microperoxidase-8[9] and microperoxidase-11,[10] heme-binding four-helix bundle,[11] synthetic multiheme proteins,[12] helichrome,[13] and other synthetic model compounds[14] are examples of either covalent or noncovalent heme–peptide complexes.

In this paper we describe the design, synthesis, and spectroscopic characterization of the first representative of such peptide–heme adducts, named mimochrome I. The free base, 3,7,12,17-tetramethylporphyrin-2,18-di-N_{ε}-(Ac–Leu^1–Ala^2–Gln^3–Leu^4–His^5–Ala^6–Asn^7–Lys^8–Leu^9–NH_2)propionamide, is depicted in Figure 1. It contains deuteroporphyrin bound through both propionyl groups to two identical *N*- and *C*-terminal protected nonapeptides as α-helical scaffolds. Each peptide moiety bears a His residue in the central position that may act as an axial ligand in the derivative encapsulating the metal ion. We describe here the newly developed general strategy that allows a facile synthesis of a large variety of analogues containing either symmetric or unsymmetric peptide chains covalently bound to the deuteroporphyrin ring. The synthetic strategy employing deuteroporphyrin also permits the subsequent insertion of various metal ions. The iron(III) derivative was easily synthesized. UV/Visible spectra, coupled with CD measurements, in TFE/water buffered solutions confirm the designed hypothetical model regarding both the iron(III) coordination and the peptide chain structural organization. Evidence of the origin of the induced Cotton effect in the Soret region is also reported here. Spectroscopic characterization in different media by NMR, EPR, and resonance Raman and a preliminary description of binding properties and reactivity of Fe^{III} mimochrome I appear in the following paper. Preliminary accounts of the design, synthesis, and characterization of Fe^{III} mimochrome I have already appeared.[15]

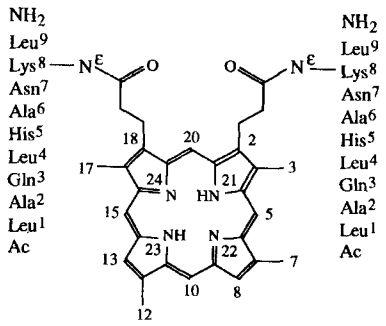

Figure 1. Schematic structure of mimochrome I with the numbering scheme adopted.

The aim of our work is, in summary, the development of a new class of peptide-based hemoprotein mimetic characterized by conformationally well-organized peptide chains. Their structures should be preserved upon metal-ion axial coordination. A rigid three-dimensional structure will allow a more detailed understanding of the structure–activity relationship. A well-defined peptide conformation might also function as template structure for the binding of specific substrates. This selective recognition constitutes a key step in the development of highly stereo- and chemoselective synthetic catalysts.

Abstract in Italian: *In questo lavoro sono riportati la progettazione, la sintesi e la caratterizzazione spettroscopica di una nuova molecola, denominata mimochrome I, costituita da un "sandwich" covalente elica–eme–elica. Essa contiene la deuteroemina, i cui gruppi propionici sono legati a due identici nonapeptidi, protetti alle estremità N- e C-terminali, tali da stabilizzare strutture elicoidali. Ogni catena peptidica presenta in posizione centrale un residuo di His quale legante assiale per il metallo inserito nel nucleo porfirinico. La nuova strategia sintetica sviluppata si basa sia su metodologie in soluzione che in fase solida. Essa rappresenta un utile metodo per ottenere una grande varietà di analoghi, costituiti da catene peptidiche simmetriche o asimmetriche legate covalentemente all'anello deuteroporfirinico. La caratterizzazione mediante spettroscopia UV/visibile in soluzioni 2,2,2-trifluoroetanolo/tampone fosfato mostra una biscoordinazione delle due His allo ione Fe^{III}, che assume uno stato di basso spin; misure di dicroismo circolare mostrano una conformazione α-elicoidale per i due segmenti peptidici. Tutti i risultati sperimentali confermano il modello ipotetico progettato, sia per quanto riguarda la coordinazione allo ione metallico che per l'organizzazione strutturale delle catene peptidiche.*

Abbreviations used for natural amino acids and peptides are those of the IUPAC-IUB Commission on Biochemical Nomenclature (IUPAC-IUB, 1984, 1989); TFA, trifluoroacetic acid; PyBop, benzotriazol-1-yloxytris(pyrrolidino)phosphonium hexafluorophosphate; HOBt, 1-hydroxybenzotriazole; NMM, *N*-methylmorpholine; DMF, dimethylformamide; Fmoc, 9-fluorenylmethoxycarbonyl; *t*Boc, *tert*-butoxycarbonyl; OPfp, pentafluorophenyl ester; DCM, dichloromethane; DIEA, diisopropylethylamine; DMSO, dimethyl sulfoxide; Dde, 1-(4,4-dimethyl-2,6-dioxocyclohexylidene)ethyl; Trt, triphenylmethyl; TFE, 2,2,2-trifluoroethanol.

Results and Discussion

Peptide design: We performed a detailed analysis of the known X-ray structure of heme-binding proteins before designing mimochrome I. Several hemoproteins, such as cyto-

chrome P450,[16a,b] cytochrome c,[17], cytochrome $c3$,[18] and cytochrome b,[19] exhibit irregular folding of their protein chain in close proximity to the heme. In contrast, hemoglobin,[20] myoglobin,[21] cytochrome c',[22] and cytochrome $b562$[23] are characterized by a heme group almost completely embedded between two relatively small α-helical peptide segments. We used these hemoproteins as template structures. They have the following features: a) a minimum nine- or ten-residue α-helical peptide segment is required for a complete coating of one face of the heme group, b) the potential iron axial ligand is located approximately at the central position of the nonapeptide sequence, c) hydrophobic residues surround the axial coordinating residue and they face the heme directly, d) the remaining five/six helical residues point outward from the heme group, and e) one peptide helix axis is about parallel to the heme plane.

Figure 2a shows the β-chain F helix facing the heme group taken from the X-ray structure of human deoxyhemoglobin.[20]

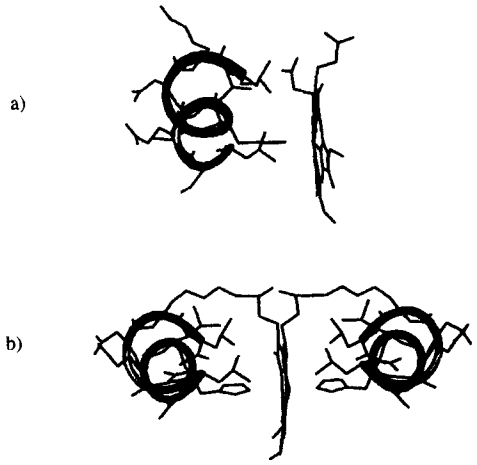

Figure 2. a) X-ray structure of β-chain Leu^{88}–Leu^{96} F helix fragment facing the heme group in deoxyhemoglobin; b) possible structure of Fe^{III} mimochrome I designed from molecular graphic studies. The ribbon structure is also reported to display the helical structure.

Simple molecular modeling studies showed that a change of the conformation of the heme propionyl group and of the Lys^{95} sidechain from a folded state to an extended state would allow us to bring the propionyl carboxy moiety and the lysine ε-amino functional group to bonding distance. This covalent bridge appeared to be a minimum requirement for positioning the helical scaffold in good proximity to the iron center and for driving the peptide chain to cover the heme face upon His axial coordination. N-terminal acetylation and C-terminal amidation were then stipulated to avoid the presence of end charges that might affect the helix stability. Residues Ser^{89}, Glu^{90}, Cys^{93}, and Asp^{94} were replaced with Ala, Gln, Ala, and Asn, respectively, in order to simplify the synthetic procedure. The resulting sequence appeared to have a high propensity to assume the desired helical folding, owing to the presence of five helix-inducing residues ($Leu^{1,4,9}$, $Ala^{2,6}$) in a peptide of nine residues and to the N- and C-terminal protection.[24] Deuteroporphyrin was preferred to the more common protoporphyrin IX to avoid the possibility of degradation of the sensitive vinyl substituents during the synthesis. Finally, the helix–heme–helix sandwich, shown in Figure 2b and obtained by applying a C_2 symmetry operation, was designed as a first target. It must, however, be considered that, owing to the linker flexibility between the peptide and the deuteroporphyrin ring, two different orientations of the peptide chains are possible. In fact, each peptide chain can be arranged above or below the porphyrin plane, giving rise to enantiomeric configurations around the Fe^{III} center. This is schematically depicted in Figure 3.

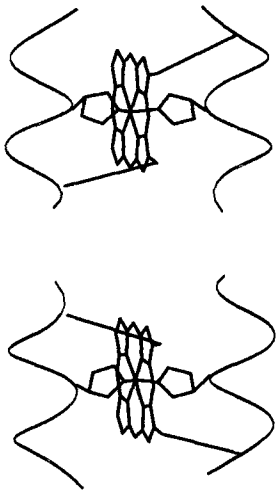

Figure 3. Schematic representation of the two possible diastereomers for Fe^{III} mimochrome I.

Synthesis: Mimochrome I was synthesized by means of both solution and solid-phase peptide methods. Scheme 1 reports the synthetic procedure developed. The classical N-α-Fmoc protocol was used;[25] all amino acids, except α-Dde–Lys–(ε-Fmoc)–OH, were used as pentafluorophenyl esters and activated to HOBt esters; α-Dde–Lys–(ε-Fmoc)–OH was coupled according to the pyBop/HOBt procedure.[26] The synthesis of the dipeptide Fmoc–Lys–Leu–NH_2 (**2**) and its coupling to deuteroporphyrin IX were performed in solution. The monosubstituted deuteroporphyrin IX–dipeptide molecule (**3**) was then linked through the free propionic group to the ε-amino function of the Lys–Leu

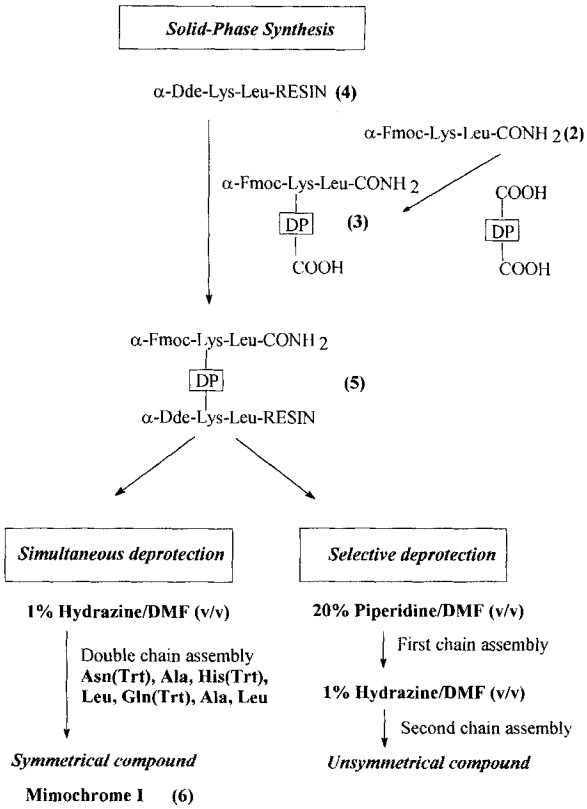

Scheme 1. Schematic presentation of the synthetic procedure.

0947-6539/97/0303-0342 $ 15.00+.25/0 Chem. Eur. J. 1997, 3, No. 3

dipeptide anchored to the solid support **4**. A negative Kaiser test[27] at this point demonstrated completeness of the coupling, since the presence of the porphyrin does not affect the result of the test. As further evidence, analysis of the crude material obtained after completion of the peptide assembly showed no peptide product lacking in the porphyrin moiety.

After completion of the molecular assembly on the resin and cleavage by treatment with acid, iron(III) was inserted overnight by means of iron(II) acetate in a mixture of acetic acid and trifluoroethanol as solvent. The overall yield of the complex purified by reverse-phase HPLC was 56%. FAB mass spectrometry gave a molecular ion peak $[M - H^+]$ of 2623, corresponding to the expected value for Fe^{II} mimochrome I.

The use of two orthogonal amino protecting groups, Fmoc and Dde, for the α-amino functions of the two Lys residues leads to two synthetic routes starting from compound **5**. The synthesis of two identical peptide sequences can be achieved by the simultaneous cleavage of Fmoc and Dde with hydrazine,[28] as was performed in the preparation of mimochrome I. Alternatively, selective Fmoc cleavage with piperidine allows the synthesis of a single peptide chain. The subsequent cleavage of the Dde group by hydrazine allows the assembly of the second peptide chain. Thus, a molecule with two different peptide sequences linked to the porphyrin ring can be synthesized. Moreover, the use of a metal-free porphyrin derivative makes this synthetic strategy very useful for a fast screening of the effect that the peptide scaffold has on the properties of different metal ions.

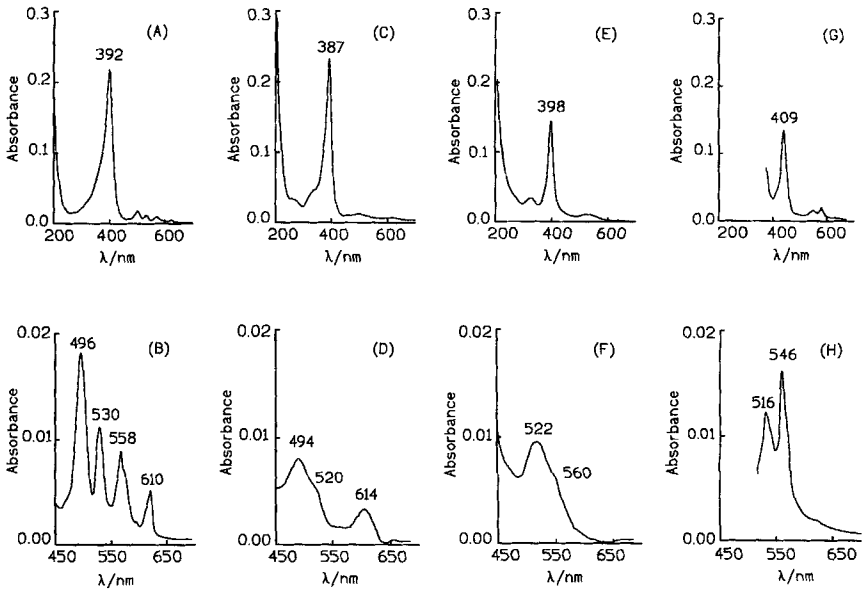

Figure 4. UV/Vis spectra in TFE/water solution (1:1 v/v): (A) and (B): mimochrome I in the Soret and visible regions, respectively; (C) and (D): ferric mimochrome I at pH 2 in the Soret and visible regions, respectively; (E) and (F): ferric mimochrome I at pH 7 in the Soret and visible regions, respectively; (G) and (H): ferrous mimochrome I at pH 7 in the Soret and visible regions, respectively.

UV/Visible spectral properties: In order to confirm the iron insertion into mimochrome I and to investigate the coordination geometry of the metal ion, several UV/visible spectra in TFE/water buffered solutions were recorded.

Table 1 summarizes the UV/Vis spectral data of mimochrome I and Fe^{III}/Fe^{II} mimochrome I. The UV/Vis spectra in TFE/water (1:1) of mimochrome I at pH 7.0, ferric mimochrome I at pH 2.0 and pH 7.0, and ferrous mimochrome I at pH 7.0 are shown in Figure 4. As a consequence of the limited solubility in aqueous solution, all spectra were recorded in aqueous buffer solutions containing TFE, which is commonly used for peptide structural characterization in solution. The linear correlation between absorbance and concentration indicated negligible association phenomena in a concentration range over three orders of magnitude (10^{-8}–10^{-5} M). Aggregation phenomena were observed only at concentrations higher than 2.0×10^{-5} M. The red shift of the Soret band from 392 to 398 nm in TFE/phosphate buffer at pH 7 (entries 1 and 3 in Table 1), together with the replacement of the four low-energy bands (β and α) by a single band at about 522 nm and a shoulder at about 560 nm in both solvent systems, clearly indicated the metallation of porphyrin ring by the iron(III) ion.[29]

Table 1. UV/Visible spectral data of mimochrome I in TFE/water (1:1).

Species	pH	UV/Vis λ_{max}, nm Soret	β	α
1, mimochrome I	7.0	392	496–530	558–610
2, ferric mimochrome I	2.0	387	494–520(sh)	614
3, ferric mimochrome I	7.0	398	522–560(sh)	
4, ferrous mimochrome I	7.0	409	516	546

In order to understand the coordination geometry and the spin state of ferric mimochrome I, the effect of pH on the UV/Vis spectra was evaluated. At very acidic pH (≈2), the spectrum of ferric mimochrome I is characterized by a blue-shifted Soret band and β/α bands located around 500 and 615 nm. These spectral features are in agreement with a high spin state characterized by two weak axial ligands on the iron (i.e., water molecules).[30] In these conditions it is reasonable to believe that both histidine residues are protonated and unable to coordinate the iron ion. At neutral pH, where presumably both histidine residues are deprotonated and able to bind the iron atom, the Soret band is red-shifted, the α band around 620 nm disappears, and a shoulder around 560 nm appears. Bis(histidine) axial coordination with low spin state can be inferred.[31]

pH titration in TFE/phosphate buffer (1:9 v/v) from pH 7 to pH 2 causes a blue shift of the Soret band from 398 to 387 nm and the splitting of the α/β region into two bands (Figure 5). This behavior can be interpreted in terms of protonation and displacement of the axial ligands around pH 2.5. The unexpectedly low value of the His pK_a is also in agreement with a low-spin hexacoordinated complex as major component in the analyzed solvent system, and strongly supports the hypothetical structure proposed for Fe^{III} mimochrome I. The leucine sidechains surrounding the histidine residue create a highly hydrophobic local environment, which lowers the histidine pK_a. The hydrophobic interactions between the leucine sidechains

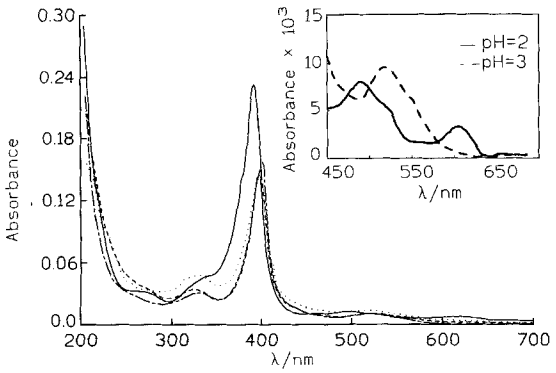

Figure 5. UV/Vis pH titration in TFE/phosphate solutions (1:9 v/v) of ferric mimochrome I. Inset: Changes in the visible region on an expanded scale.

and the deuterohemin ring further favor the imidazole–iron coordination.

Ferrous mimochrome I was obtained by adding deaerated concentrated dithionite solutions directly to deaerated solutions of ferric mimochrome I in the spectrophotometric cuvettes. UV/Visible spectra of ferrous mimochrome I in TFE/water solution (Table 1 and Figure 4) show the expected red shift of the Soret band that is usually found upon reduction of the metal center in porphyrin systems. The Soret band energy is in good agreement with bis(histidine) iron(II) axial coordination.[32] The visible regions of the spectra are more sensitive to the axial coordination of iron(II). The presence of two bands observed in our case, with higher intensity for the band at higher wavelength, is diagnostic for coordination of two histidine residues on the iron(II) axial positions.[30]

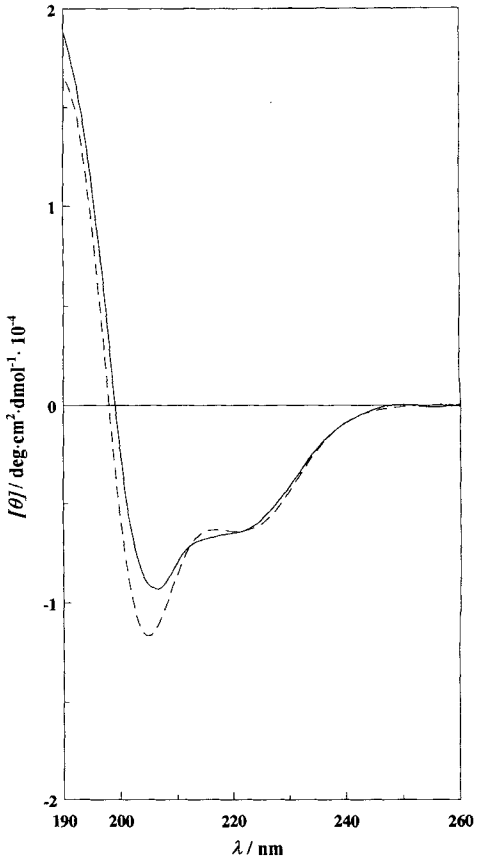

Figure 6. UV region CD spectra in TFE/water solution (1:1 v/v); — mimochrome I at pH = 7; - - - ferric mimochrome I at pH = 7. [θ] is expressed as mean residue ellipticity.

Far-UV CD spectra: Circular dichroism measurements in TFE/water solutions for both mimochrome I and ferric mimochrome I were recorded in the 260–190 nm region. Figure 6 shows the CD spectrum of mimochrome I and ferric mimochrome I, pH = 7, in 50% TFE/water. Table 2 reports the typical CD parameters.

The double minima at 222 and 205 nm as well as the maximum at about 190 nm indicate the peptides to be predominantly in a helical conformation.[33] The ellipticity at 222 nm is the most commonly used parameter to describe helix formation. Theoretical calculations have indeed suggested that this value is very sensitive to both the length of the helix and to the local conformation of each residue.[34] Although the $[\theta]_{222}$ value can be correctly applied to calculate the helix percentage in proteins, it fails in estimating the helix contents in small peptides. Vuillemier and Mutter[35] reported that in small peptides three spectral parameters are significant in revealing helix propensity: a) the [θ] ratio of the minimum at 222 nm to the minimum at shorter wavelengths, b) the position of this last minimum, c) the crossover wavelength λ_0. In particular, an increase of the [θ] ratio to a value around unity, together with a shift of the shorter wavelength minimum toward 207 nm and a shift of the λ_0 value to longer wavelengths are indicative parameters of high helix propensity. As shown in Table 2 and Figure 6, mimochrome I and ferric mimochrome I at pH 7 have quite similar $[\theta]_{222}$ and λ_0 values, which are indicative of an equal helix con-

Table 2. CD parameters of mimochrome I in TFE/water solutions [a].

Species	% TFE	$[\theta]_{min} \times 10^{-3}$ [b] (λ_{min}, nm)	$[\theta]_{222} \times 10^{-3}$	$[\theta]_{ratio}$ [b]	λ_0, nm	$[\theta]_{190} \times 10^{-3}$	$[\theta]_{395} \times 10^{-3}$ [c]	$[\theta]_{410} \times 10^{-3}$
UV region								
Fe^{III} mimochrome I	50	−11.7 (204.8)	−6.4	0.55	198.1	16.7		
mimochrome I	50	−9.3 (206.2)	−6.4	0.70	199.1	18.7		
Soret region								
Fe^{III} mimochrome I	10						−19.7	–
Fe^{III} mimochrome I	20						−24.5	–
Fe^{III} mimochrome I	50						−17.7	1.2
Fe^{III} mimochrome I	100						−11.1	5.4 (407.6) [d]

[a] Parameters are derived from the experimental CD spectra recorded under the conditions indicated in the experimental section; pH 7. [b] In the UV region [θ] is expressed as mean residue ellipticity (°cm² dmol⁻¹), calculated by dividing the total molar ellipticities by the number of amino acids in the molecule; [θ] ratio represents the ratio of the ellipticity at 222 nm to that at the shorter wavelength minimum. [c] [θ] in the Soret region is reported as total molar ellipticity. [d] λ_{max} is reported in parenthesis.

0947-6539/97/0303-0344 $ 15.00+.25/0 Chem. Eur. J. 1997, 3, No. 3

tent, but the $[\theta]$ ratio changes from 0.70 in the free base to 0.55 in the iron(III) complex. This difference probably denotes a distortion in the α-helix induced by the coordination of the His residues to the metal ion. It has been reported that 3_{10}-helices should display a more intense minimum in the 207 nm region, lowering the $[\theta]$ ratio;[34c] and thus a conformational transition from α-helix to 3_{10}-helix upon coordination could be suggested. However, we cannot exclude the possibility that the changes in the far-UV CD spectra may derive from the interactions between the heme transitions and those of the peptide backbone amide dipoles.[14e, 36]

The effect of the helix-inducing solvent TFE[37] on the CD spectral features of ferric mimochrome I was also investigated (Figure 7). As expected, the peptide chains adopt a helical conformation, even at low TFE concentration (10%), and the helix content increases upon increasing the TFE content (up to 30%).

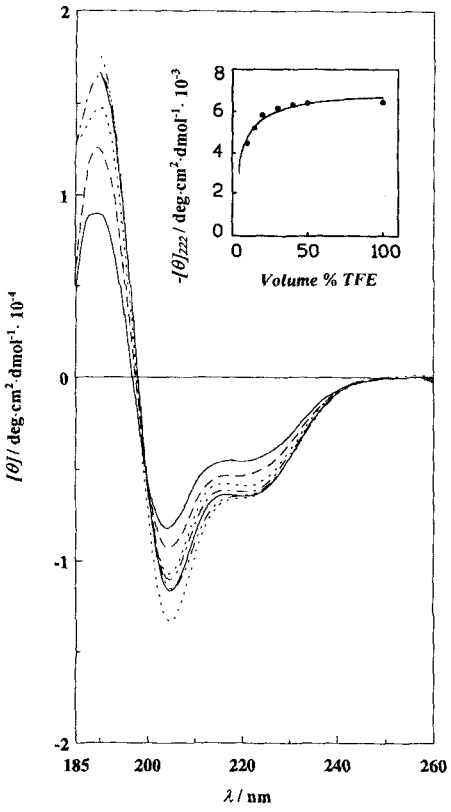

Figure 7. UV region CD spectra of ferric mimochrome I in buffered solutions (pH 7) at different TFE concentrations. Inset: titration curve showing θ_{222} as a function of TFE concentration.

The inset in Figure 7 reports the θ_{222} value as a function of TFE concentration.

Soret region CD spectra: The CD features of ferric mimochrome I were also investigated in the 400 nm region. As can be seen from Figure 8, the shape and the intensity of the induced Cotton effect in the Soret band is related to the solvent composition. At low TFE concentrations (< 20% v/v), the CD spectra are characterized by a strong negative peak, centered at 395 nm, the intensity of which is increased by increasing the TFE concentration (from 19.7×10^3 to 24.5×10^3 ° cm^2 dmol^{-1}). An opposite behavior is observed from 20% to 100% TFE concentration. In fact, the induced Cotton effect decreases in intensity (from 24.5×10^3 to 11.1×10^3 ° cm^2 dmol^{-1}) and it goes toward a doubly inflected shape at 50% TFE concentration. The inset in Figure 8 reports the θ_{395} value as a function of TFE concentration.

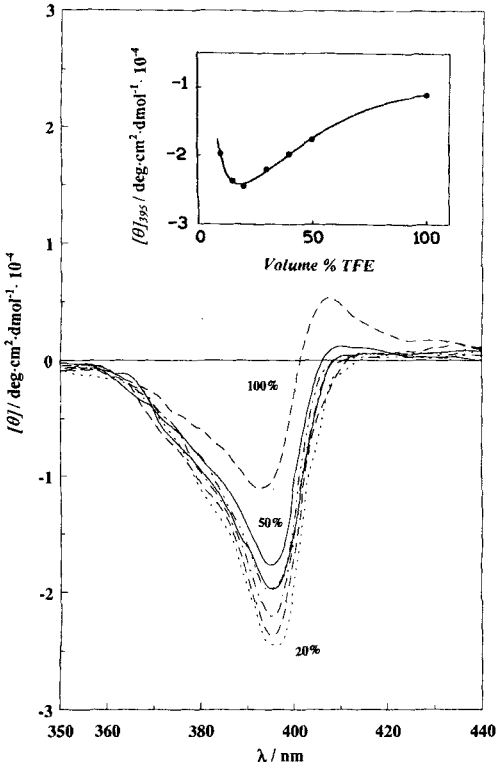

Figure 8. Soret region CD spectra of ferric mimochrome I in buffered solutions (pH 7) at different TFE concentrations. $[\theta]$ is expressed as total molar ellipticity. Inset: titration curve showing θ_{395} as a function of TFE concentration.

It has been widely reported that the protein folding around the heme chromophore is the main factor inducing optical activity in the Soret transition for hemoproteins.[38] Because of the mutual orientation of the heme and the protein, an induced Cotton effect may result from a coupling of $\pi-\pi^*$ heme transition with $\pi-\pi^*$ and $n-\pi^*$ transitions localized in the polypeptide backbone or $\pi-\pi^*$ transitions of aromatic sidechains. Theoretical studies[39] have shown that the shape of the heme $\pi-\pi^*$ Cotton effects depends upon the direction of polarization of the Soret components in the heme plane. However, the shape and the complexity of the Soret–Cotton effect cannot be easily related to the protein conformation and structural organization. In fact, different shapes of the Cotton effect can be observed in hemoproteins containing identical heme groups and characterized by an overall similar structure; changes may occur by several mechanisms, such as binding of certain ligands, mixing of the porphyrin transitions with those of the metal atom, and nonplanarity of the porphyrin ring. For example, myoglobin and legemoglobin are both characterized by strong Soret–Cotton effects, but it is surprising that their magnitudes are of the same order even though of opposite sign.[40] Consequently, the interpretation of the Soret-induced Cotton effect shown by ferric mimochrome I in comparison with literature data on heme-binding proteins is rather difficult; moreover, detailed informa-

tion on the His sidechains and helix axis orientation with respect to the porphyrin ring for ferric mimochrome I are not available. The CD effect in the Soret region will be better clarified once a complete description of its three-dimensional structure has been obtained. For this purpose, we synthesized Co^{III} mimochrome I, which has been fully characterized by ^1H NMR spectroscopy (see the following paper).

However, the shape of the curve relating θ_{395} to the TFE concentration indicates the occurrence of two different phenomena (see the inset in Figure 8). With the assumption that the induced Cotton effect may result from a coupling of $\pi-\pi^*$ heme transition with $\pi-\pi^*$ and $n-\pi^*$ transitions localized in the polypeptide backbone, it is reasonable to hypothesize that the increase in intensity of the Soret-induced Cotton effect at TFE concentration up to 20% is related to the increase in helical content (Figure 9). At TFE concentrations higher than 20% the

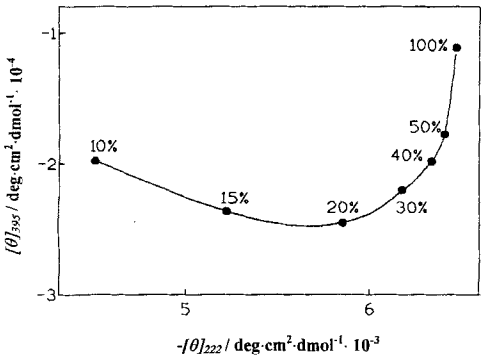

Figure 9. Plot of θ_{395} vs. θ_{222} for ferric mimochrome I in buffered solutions (pH 7) at different TFE concentrations. $[\theta]_{395}$ and $[\theta]_{222}$ are expressed as total molar ellipticity and mean residue ellipticity, respectively.

helical content increases slightly, but the intensity of the induced Cotton effect at 395 nm decreases. This unexpected behavior can tentatively be attributed to the appearance of a diastereomeric form, the molar fraction of which increases when the TFE concentration is increased. This isomer, as mentioned in the design section, would be characterized by an enantiomeric orientation of the peptide chains with respect to the deuteroporphyrin ring and therefore an opposite-sign Cotton effect may be induced. The observed effect at high TFE concentrations could be interpreted as the sum of the two opposite diastereomeric contributions. In summary, it seems to us that at low TFE concentration one diastereomeric form is present as the major component, and a small increase in TFE concentration mainly produces an increase in the helical content of the peptide chains. Consequently, an increase in the intensity of the induced Cotton effect at 395 nm is observed. Higher TFE concentrations also cause a transition toward the formation of a distereomeric form, which is characterized by a positive induced Cotton effect in the Soret region. This hypothesis agrees well with our findings on the Co^{III} mimochrome I derivative, described in the following paper, but it certainly requires further experimental evidence to be considered proven.

The splitting into two opposite bands of the CD Soret band (S-shaped) that appear for Fe^{III} mimochrome I at 50% TFE concentration is in agreement with the previous observations and can be related to the interconversion between the two isomers. Different positions of the maxima, different shapes, and different intensities in the Soret-region Cotton effect of the diastereomeric forms may give an overall S-shaped spectrum. However, the S-shaped spectrum can also be characteristic of exciton splitting resulting from heme–heme interaction.[38] This arrangement cannot be inferred for Fe^{III} mimochrome I, since it is a one-heme-per-molecule system and aggregation phenomena are absent, as proven by the linear correlation between absorbance and concentration in a wide range (10^{-8}–10^{-5} M). Moreover, it should be mentioned that S-shaped spectra have also been reported for bis-coordinated hemoproteins with different axial ligands (His and Met), such as ferricytochrome c[41] and cytochrome b-562.[42] Therefore, we cannot exclude the possibility that an unsymmetrical axial ligation around the iron(III) center may be present at higher TFE concentration, which in turn may produce a small S-shaped Cotton effect. Furthermore, the distortion of the heme ring as the TFE concentration is increased may also provide a reasonable explanation for the observed phenomena; however, the NMR spectra of both Δ and Λ diastereomers of Co^{III} mimochrome I do not provide information on the twist of the porphyrin ring (see part 2 following).

In our opinion, our results are also in agreement with the studies reported in ref. [14e]. The authors proposed that the designed peptide-sandwiched mesoheme exists as a pair of interconvertible diastereomers, and their model system is characterized by a negative CD band in the Soret region, whose intensity decreases as both the TFE concentration and the temperature are increased. From the hypothesis that the CD Soret band intensity is a function of the peptide conformation only, an increase in temperature should have the opposite effect to an increase in TFE concentration. Therefore, the induced Cotton effect in the Soret region for the sandwiched mesoheme described by Benson et al. decreases when the temperature is increased, as a consequence of peptide unfolding; in contrast, the same compound shows a decrease in the Soret–Cotton effect when the TFE concentration is increased, because a diastereomeric form is appearing.

Conclusions

Mimochrome I is the prototype of a new class of low-molecular-weight hemoprotein models. The main feature of mimochrome I is the covalent structure and the well-defined helical conformation of the peptide chains. In our design we considered that the prosthetic group in natural hemoproteins is kept firmly inside the protein structure by a large number of interactions responsible for protein folding; these interactions can be replaced in low-molecular-weight models by a few strong local constraints. By a detailed analysis of hemoprotein structures we were able to identify the smallest peptide sequence (nine residues) required for complete coverage of one face of the heme group, and we also found that the α-helical conformation is a common feature among many hemoprotein structures. By the use of the F helix of the hemoglobin β-chain as a template structure, we designed a peptide sequence which, rather surprisingly, retains the α-helical conformation even in the absence of the entire protein struc-

0947-6539/97/0303-0346 $ 15.00+.25/0 Chem. Eur. J. 1997, 3, No. 3

ture, both in the metal-free compound and in its iron derivative. This behavior makes our model compound unique and quite different from a recently developed peptide-sandwiched meso-heme derivative,[14e] which represents a conformationally flexible system where the peptide chain folding, from a completely random coil into a helical conformation, is induced by histidines coordinating to iron. Our design strategy is, thus, of great scientific relevance because it leads to the structure of mimochrome 1 which, when compared with other reported molecules,[14e] is less dependent on the environment and on metal binding. Furthermore, our design is, to the best of our knowledge, the first example of a minimalist approach which uses a protein structure as reference object. It differs from previous works, reported for example by Choma et al.[11] and by Benson et al.,[14e] in which de novo designed helical peptides were used to bind a heme group covalently[14e] or noncovalently.[11]

The general versatile and novel strategy for the synthesis of helix–heme–helix sandwiches in high yields described in the present paper permits rapid preparation of a large variety of analogues with either symmetric or unsymmetric peptide chains. To the best of our knowledge, this is the first example of porphyrin-derivative incorporation on a solid support based on Fmoc chemistry, which proves the stability of the deuteroporphyrin ring in all the synthetic steps. Since the metallation reaction is performed on the assembled peptide–porphyrin moiety, the incorporation of different metal ions in the porphyrin ring is possible without resynthesizing the entire molecule, thus opening new opportunities for easy and fast screening of a wide variety of metal complexes.

UV/Visible spectroscopy and CD measurements corroborated the hypothetical structure of Fe^{III} mimochrome I, suggesting that it exists predominantly in a low-spin hexacoordinated state, with His–Fe^{III}–His axial ligation. CD measurements in the far UV region confirmed the peptide chain to be mainly α-helical in both the *apo* and metallated species. The behavior of the induced Cotton effect in the Soret region can tentatively be ascribed both to the peptide helical content and to the simultaneous presence of the two diastereomeric forms, whose ratio depends on the TFE concentration. This hypothesis is supported by the properties of the Co^{III} mimochrome I complex, which exists in solution as two diastereomers; it was possible to isolate and to characterize separately these two isomers for the cobalt derivative, which was not the case for the iron complex. Unfortunately, the spectroscopic techniques employed here cannot provide compelling proof that the structure of the iron complex is as designed, but a detailed characterization by NMR spectroscopy, of the more soluble Co^{III} mimochrome I analogue fully confirms our hypothetical model, and is presented in the next paper.

Experimental Procedure

Design: Molecular design was performed on a Silicon Graphics workstation Personal Iris 4D/35 GT TURBO; X-ray structural data for human deoxyhemoglobin[20] from the Protein Data Bank, Brookhaven National Laboratory (Upton, NY, USA),[43] and the Insight program package (Biosym) were used.

Synthesis equipment and materials: The synthesis of mimochrome I was achieved on a Milligen 9050 automatic peptide synthesizer. Analytical reverse-phase high-performance liquid chromatography (RP-HPLC) was performed on a Varian 3000 LC Star System, equipped with a 9065 Polychrom and a 9095 AutoSampler. A Vydac C_{18} column (4.6 × 150 mm; 5 μm), eluted with a H_2O/0.1% TFA (A) and CH_3CN/0.1% TFA (B) linear gradient, from 20 to 80% B over 25 min, at 1 mL min^{-1} flow rate, was used in all analysis. A Waters Delta Prep 3000 HPLC, equipped with an UV Lambda-Max Mod 481 detector, was used for the purification of the products. A linear gradient from 20 to 80% of B over 40 min at flow rate of 114 mL min^{-1}, on a Vydac C_{18} column (50 × 250 mm; 10 μm) was employed in all purification. FAB mass spectra were obtained with a VG ZAB2SE double-focusing mass spectrometer equipped with a cesium gun operating at 25 kV (2 μA) at the Servizio di Spettrometria di Massa, CNR Università di Napoli. ^{1}H NMR 1D and 2D experiments were recorded on a Varian Unity 400 spectrometer, operating at 400 MHz and equipped with a Sparc Station SUN 330.

All amino acids, the resin, pyBop and HOBt were purchased from Nova Biochem; NMM, piperidine and scavengers were from Fluka, TFA from Applied BioSystems. All solvents used in the peptide synthesis and purification were anhydrous and HPLC grade, respectively, and were supplied by LabScan Analytica. Deuteroporphyrin IX was from Porphyrin Products. Iron(II) acetate was from Aldrich. Deuterated [D_6]DMSO was from Cambridge Isotope Laboratories (99.96% relative isotopic abundance). Silica gel 60 (230–400 mesh) was from Merck. Precoated silica G-60 plates, F254 (Merck) were used for thin-layer chromatography (tlc). Solvent mixtures are indicated in the respective sections. For product identification, ninhydrin, iodine vapor staining or fluorescence detection were used.

Fmoc–Lys–(ε-Boc)–Leu–NH_2 (1): HOBt (0.891 g, 6.6 mmol) and Fmoc–Lys–(ε-Boc)–OPfp (3.8 g, 6 mmol), both dissolved in DMF (6 mL), were added to a solution containing H–Leu–NH_2·HCl (1.1 g, 6 mmol) and NMM (0.771 mL, 6.9 mmol) in DMF (6 mL). The reaction mixture was stirred for 1 h at room temperature. The solvent was evaporated under vacuum and the foamy residue was triturated with a saturated citric acid solution, water, saturated $NaHCO_3$, and finally with water. The product was dried under vacuum over P_2O_5, affording 3.31 g (yield 95%) of a white powder, pure on tlc. $R_f = 0.7$ in acetonitrile. RP-HPLC $R_t = 18.35$ min.

Fmoc–Lys–Leu–NH_2 (2): Boc cleavage was achieved by treatment of **1** (2.3 g, 4 mmol) with a 33% TFA solution in DCM (24 mL) for 18 min. Precipitation of the product as TFA salt occurred after solution concentration and addition of diethyl ether. Yield 100%. $R_f = 0.59$ in chloroform/methanol/acetic acid 8:1.8:0.2.

3,7,12,17-tetramethylporphyrin-18(2)-propionic acid-2(18)-N_1ε-(α-Fmoc–Lys^1–Leu^2–NH_2)propionamide (3): DIEA (0.713 mL, 4.28 mmol), dipeptide **2** (0.508 g, 0.856 mmol), dissolved in DMF (42.5 mL), were added to a solution containing deuteroporphyrin IX (0.500 g, 0.856 mmol) in DMF (85 mL). Finally pyBop (0.445 g, 0.856 mmol), dissolved in DMF (42.5 mL), were added dropwise. The reaction mixture was stirred for 2 h at room temperature. The solvent was removed under vacuum, and the crude product was purified on a silica gel column (60 × 500 mm), with stepwise elution with a chloroform/methanol mixture from 0 to 20% methanol. The most abundant product was eluted with the 20% methanol mixture; yield: 68%. $R_f = 0.26$ in chloroform/methanol 90:10. ^{1}H NMR analysis identified this product as the desired product. ^{1}H NMR (400 MHz, [D_6]DMSO, 25 °C, TMS): $\delta = -4.00$ (s, 2H, *21,23* NH), 0.78, 0.81 (d, 6H, δ-CH_3 Leu^2), 1.10 (br, 2H, δ-CH_2 Lys^1), 1.35 (br, 3H, β-CH_2–γ-CH Leu^2), 1.45 (br, 4H, β-CH_2, γ-CH_2 Lys^1), 2.95 (br, 2H, ε-CH_2 Lys^1), 3.03 (br, 2H, α-CH_2 *2(18)* propionamide), 3.12 (br, 1H, CH Fmoc), 3.15 (br, 2H, α-CH_2 *18(2)* propionic acid), 3.61, 3.62, 3.65, 3.66, 3.74, 3.77 (6s, 12H, *3,7,12,17* CH_3), 3.90 (br, 1H, α-CH Lys^1), 4.10 (d, 2H, CH_2 Fmoc), 4.20 (br, 1H, α-CH Leu^2), 4.38 (br, 4H, β-CH_2 *2(18)* propionamide–*18(2)* propionic acid), 6.95, 7.30 (2s, 2H, $CONH_2$ Leu^2), 7.32, 7.42 (2d, 4H, Fmoc), 7.70, 7.90 (2t, 4H, Fmoc), 7.50 (d, 1H, NH Lys^1), 7.84 (d, 1H, NH Leu^2), 8.04 (t, 1H, ε-NH Lys^1), 9.30, 9.35 (2s, 2H, *8,13* CH), 10.34, 10.30 (br, 4H, *5,10,15,20* CH).

(α-Dde)–Lys–Leu–resin (4): The dipeptide was synthesized by means of the Fmoc strategy in continuous-flow solid-phase peptide synthesis[25] on NovaSyn PR 500 resin (substitution 0.5 mmol g^{-1}; 0.2 mmol scale). The Fmoc–Leu derivative was used as pentafluorophenyl active ester; 4 equiv amino acid, dissolved in a 0.3 M HOBt solution in DMF, were used in the coupling step (acylation time: 30 min). Lys was inserted as (α-Dde)–Lys–(ε-Fmoc)–OH and coupled according to the pyBop procedure:[26] 4 equiv Fmoc–

amino acid, 4 equiv pyBop and 8 equiv DIEA in DMF (acylation time: 2 h). Each coupling step was repeated twice. Completeness of the reaction was checked after each coupling by the Kaiser test.[27] Fmoc protecting group was removed by piperidine in DMF (20% v/v; 3 + 7 min).

3,7,12,17-tetramethylporphyrin-2(18)-$N_1\varepsilon$-(α-Fmoc-Lys^1-Leu^2-NH_2)-18(2)-$N_1\varepsilon$-(α-Dde-Lys^1-Leu^2-resin)dipropionamide (5): The deuteroporphyrin dipeptide **3** was coupled to the dipeptidyl resin **4** manually: **3** (0.973 g, 0.1 mmol), pyBop (0.520 g, 0.1 mmol), and DIEA (0.033 mL, 0.2 mmol) were added to 0.1 mmol of **4** suspended in DMF. Two coupling steps of 12 and 5 h, respectively, were performed. Completeness of the reaction was checked by the Kaiser test.[27]

3,7,12,17-tetramethylporphyrin-2,18-di-$N_8\varepsilon$-(Ac-Leu^1-Ala^2-Gln^3-Leu^4-His^5-Ala^6-Asn^7-Lys^8-Leu^9-NH_2)propionamide (mimochrome I, 6): Fmoc and Dde protecting groups were removed simultaneously from **5** with hydrazine monohydrate in DMF solution (15 mL, 1% v/v, 5 min).[28] The synthesis of mimochrome I was continued with the automatic peptide synthesizer in continuous flow. The Trt group was used for the Asn, Gln, and His sidechain protection. All the Fmoc-amino acid derivatives were used as OPfp esters. The coupling and the Fmoc deprotection procedures were as described for compound **4**. The *N*-terminus was acetylated with acetic anhydride in DMF solution (12 mL, 20% v/v, 20 min). Sidechain deprotection with concomitant cleavage of the peptide from the resin was achieved with ethanedithiol/anisole/TFA 0.25/0.25/9.5 (v/v) at 0 °C (2 h). The peptidyl resin was filtered off, and the crude peptide was precipitated with diethyl ether. 0.187 g of crude material were obtained as red powder; yield 73% based on the resin substitution level. Analytical RP-HPLC showed a main single peak: $R_t = 16.8$ min. The crude material (0.087 g) was purified by preparative RP-HPLC; the pooled fractions containing the desired product were lyophilized, affording 0.052 g (2.0×10^{-2} mmol; yield 60%) of mimochrome I. Analytical RP-HPLC confirmed the purity of the product. Electrospray ionization mass spectrometry and capillary electrophoresis (data not shown) were also performed to better evaluate the presence of side products hidden in the HPLC analysis. FAB-MS gave a molecular ion peak $[M - H]^+$ of 2569 as expected.

Iron insertion: The iron was inserted into mimochrome I according to literature procedures.[4a] Iron(II) acetate (0.006 g, 3.8×10^{-2} mmol) was added to a solution containing crude compound **6** (0.050 g, 1.9×10^{-2} mmol) in acetic acid/TFE 6:4 (v/v, 100 mL). The reaction mixture was kept at 50 °C, refluxing under nitrogen. The reaction was monitored by tlc (solvent system *n*-butanol/acetic acid/water 4:1:2; $R_f = 0.4$) until the fluorescence completely disappeared (5 h); then the solvent was removed under vacuum. The product was purified by preparative RP-HPLC; 0.028 g (1.1×10^{-2} mmol; 56%) of pure Fe^{III} mimochrome I were obtained as the TFA salt. Analytical RP-HPLC confirmed the purity of the product; RP-HPLC $R_t = 17.7$ min. FAB-MS gave a molecular ion peak $[M - H]^+$ of 2623, corresponding to the expected value for Fe^{II} mimochrome I.

Sample preparation for spectroscopic characterization: Stock solutions of 5.0×10^{-4} M in TFE were prepared for both mimochrome I and Fe^{III} mimochrome I. These solutions were then diluted to about 1.0×10^{-5} M with phosphate (3.0×10^{-4} M final concentration) at desired pH (from 2 to 7) and with different amounts of TFE (from 10% to 50% v/v final concentration). Samples of Fe^{II} mimochrome I in TFE solutions were obtained by dilution of 100 μL of the 5.0×10^{-4} M TFE stock solution of Fe^{III} mimochrome I with TFE and aqueous concentrated sodium dithionite solution in the desired ratio. All these solutions were deaerated by argon bubbling for 2 h before use. Final concentrations were determined spectrophotometrically at Soret maximum wavelength with extinction coefficients calculated from Lambert and Beer's law.

UV/Visible spectroscopy: UV/Vis spectra were recorded on a Perkin-Elmer Lambda 7 UV spectrophotometer with 1 cm or 5 cm path length cells. Wavelength scans were performed at 25 °C from 200 to 700 nm (300-700 for ferrous complexes), with a 60 nm min^{-1} scan speed. Sample concentrations in the range 10^{-8}-10^{-5} M in all the solvents were used for the determination of the extinction coefficient at the Soret maximum wavelength. (Mimochrome I $\varepsilon_{392} = 95200\,M^{-1}cm^{-1}$; ferric mimochrome I $\varepsilon_{398} = 76200\,M^{-1}cm^{-1}$).

Circular dichroism measurements: CD measurements were obtained at 25 °C on a Jasco J-700 dichrograph calibrated with an aqueous solution of recrystallized D(+)-10-camphorsulfonic acid at 290 nm.[44] Data were collected at 0.2 nm intervals, with a 5 nm min^{-1} scan rate, a 1 nm band width and a 16 s response, from 260 to 185 nm in the UV region and from 450 to 260 nm in the Soret region; cuvette path lengths of 1 and 5 cm, respectively, were used. CD spectra were corrected by subtraction of the background solvent spectrum obtained under identical experimental conditions and smoothed for clarity. The experiments were carried out on the same solutions used for the UV/vis measurements. CD intensities in the UV region are expressed as mean residue ellipticities (°cm^{2}dmol^{-1}), calculated by dividing the total molar ellipticities by the number of amino acids in the molecule; intensities in the Soret region are reported as total molar ellipticities.

Acknowledgments: We are grateful to Dr. D. Mansuy and P. Battioni (Paris, France) for helpful discussions. This work is part of the Ph.D. thesis of Dr. Flavia Nastri and was supported by the Italian C. N. R., grant no. 113.156-14 (1994).

Received: August 5, 1996 [F430]

[1] a) B. Meunier, *Chem. Rev.* **1992**, *92*, 1411-1456; b) D. Mansuy, P. Battioni, J. P. Battioni, *Eur. J. Biochem.* **1989**, *184*, 267-285; c) D. Mansuy, *Pure Appl. Chem.* **1990**, *62*, 741-746; d) J. P. Collman, X. Zhang, V. J. Lee, E. S. Uffelman, J. I. Brauman, *Science* **1993**, *261*, 1404-1411.

[2] a) J. W. Buchler, B. Scharbert, *J. Am. Chem. Soc.* **1988**, *110*, 4272-4276; b) J. L. Sessler, B. Wang, A Harriman, *ibid.* **1993**, *115*, 10418-10419; c) H. Grennberg, S. Faizon, J. E. Backvall, *Angew. Chem. Int. Ed. Engl.* **1993**, *32*, 263-264; d) L. Sun, J. von Gersdorff, D. Niethammer, P. Tian, H. Kurreck, *ibid.* **1994**, *33*, 2318-2320.

[3] a) J. P. Collmann, R. R. Gagne, C. A. Reed, T. R. Halbert, G. Lang, W. T. Robinson, *J. Am. Chem. Soc.* **1975**, *97*, 1427-1439; b) T. G. Traylor, C. K. Chang, J. Geibel, A. Berzinis, T. Mincey, J. Cannon, *ibid.* **1979**, *101*, 6716-6731; c) K. S. Suslick, M. M. Fox, *ibid.* **1983**, *105*, 3507-3510.

[4] a) J. W. Buchler in *The Porphyrins, Vol. 1* (Ed.: D. Dolphin), Academic Press, New York, **1979**, pp. 389-483; b) F. Adar, *ibid., Vol. 3*, pp. 167-209; c) T. R. Janson, J. J. Katz, *ibid., Vol. 4*, pp. 1-59; d) G. N. La Mar, F. A. Walker, *ibid., Vol. 4*, pp. 61-157.

[5] *The Porphyrins, Vol. 7* (Ed.: D. Dolphin), Academic Press, New York, **1979**.

[6] D. S. Wuttke, H. B. Gray, *Curr. Opin. Struct. Biol.* **1993**, *3*, 555-563.

[7] a) C. Tetreau, D. Lavalette, M. Momenteau, J. Fischer, R. Weiss, *J. Am. Chem. Soc.* **1994**, *116*, 11840-11848; b) S. David, B. R. James, D. Dolphin, T. G. Traylor, M. Lopez, *ibid.* **1994**, *116*, 6-14.

[8] J. R. Lindsay Smith, in *Metalloporphyrins in Catalytic Oxidations* (Ed.: R. A. Sheldon), Marcel Dekker, New York, **1994**, pp. 325-368.

[9] P. A. Adams, M. P. Byfield, R. C. de L. Milton, J. M. Pratt, *J. Inorg. Biochem.* **1988**, *34*, 167-175.

[10] T. Mashino, S. Nakamura, M. Hirobe, *Tetrahedron Lett.* **1990**, *31*, 3163-3166.

[11] C. T. Choma, J. D. Lear, M. J. Nelson, P. L. Dutton, D. E. Robertson, W. F. DeGrado, *J. Am. Chem. Soc.* **1994**, *116*, 856-865.

[12] D. E. Robertson, R. S. Farid, C. C. Moser, J. L. Urbauer, S. E. Mulholland, R. Pidikiti, J. D. Lear, A. J. Wand, W. F. DeGrado, P. L. Dutton, *Nature* **1994**, *368*, 425-432.

[13] a) T. Sasaki, E. T. Kaiser, *J. Am. Chem. Soc.* **1989**, *111*, 380-381; b) T. Sasaki, E. T. Kaiser, *Biopolymers* **1990**, *29*, 79-88.

[14] a) L. Casella, M. Gullotti, L. De Gioia, E. Monzani, F. Chillemi, *J. Chem. Soc. Dalton Trans.* **1991**, 2945-2953; b) L. Casella, M. Gullotti, L. De Gioia, R. Bartesaghi, F. Chillemi, *ibid.* **1993**, 2233-2239; c) B. Pispisa, M. Venanzi, M. D'Alagni, *Biopolymers* **1994**, *34*, 435-442; d) Y. Ohkatsu, T. Watanabe, T. Goto, M. Wakita, *Bull. Chem. Soc. Jpn.* **1994**, *67*, 742-747; e) D. R. Benson, B. R. Hart, X. Zhu, M. B. Doughty, *J. Am. Chem. Soc.* **1995**, *117*, 8502-8510.

[15] a) F. Nastri, A. Lombardi, O. Maglio, G. Morelli, G. D'Auria, V. Pavone, C. Pedone, *Fourth Naples Workshop on Bioactive Peptides*, Capri (Italy), **1994**, 86; b) A. Lombardi, F. Nastri, O. Maglio, G. Morelli, V. Pavone, C. Pedone, P. Battioni, D. Mansuy, G. Chottard, *Metal Ions in Biological Systems, Eurobic II*, Florence (Italy), **1994**, 218; c) F. Nastri, A. Lombardi, O. Maglio, G. Morelli, G. D'Auria, C. Pedone, V. Pavone, in *Syntheses and Methodologies in Inorganic Chemistry, Vol. 5* (Eds.: S. Daolio, E. Tondello, P. A. Vigato), Photograf, Padova (Italy), **1995**, 242-245.

[16] a) T. L. Poulos, B. C. Finzel, A. J. Howard, *Biochemistry* **1986**, *25*, 5314-5322; b) T. L. Poulos, B. C. Finzel, A. J. Howard, *J. Mol. Biol.* **1987**, *195*, 687-700.

[17] D. C. Carter, K. A. Melis, S. E. O'Donnell, B. K. Burgess, W. F. Furey, Jr., B. C. Wang, C. D. Stout, *J. Mol. Biol.* **1985**, *184*, 279-295.

[18] M. Pierrot, R. Haser, M. Frey, F. Payan, J. P. Astier, *J. Biol. Chem.* **1982**, *257*, 14341-14348.

[19] F. S. Mathews, E. W. Czerwinski, P. Argos, in *The Porphyrins, Vol. 7* (Ed.: D. Dolphin), Academic Press, New York, **1979**, pp. 108-146.

[20] M. F. Perutz, S. S. Hasnain, P. J. Duke, J. L. Sessler, J. E. Hahn, *Nature* **1982**, *295*, 535-538.

[21] S. E. V. Phillips, *J. Mol. Biol.* **1980**, *142*, 531-554.

[22] B. C. Finzel, P. C. Weber, K. D. Hardman, F. R. Salemme, *J. Mol. Biol.* **1985**, *186*, 627-643.

[23] F. Lederer, A. Glatigny, P. H. Bethge, H. D. Bellamy, F. S. Mathews, *J. Mol. Biol.* **1981**, *148*, 427–448.
[24] a) K. T. O'Neil, W. F. DeGrado, *Science* **1990**, 250, 646–651; b) T. P. Creamer, G. D. Rose, *Proteins: Structure, Function and Genetics* **1994**, 19, 85–97; c) L. Serrano, A. R. Fersht, *Nature* **1989**, 342, 296–299.
[25] A. Dryland, R. C. Sheppard, *J. Chem. Soc. Perkin Trans. I* **1986**, 125–137.
[26] J. Coste, D. Le-Nguyen, B. Castro, *Tetrahedron Lett.* **1990**, *31*, 205–208.
[27] E. Kaiser, R. L. Colescott, C. D. Biossinger, P. I. Cook, *Anal. Biochem.* **1970**, *34*, 595–598.
[28] B. W. Bycroft, W. C. Chan, S. R. Chhabra, N. D. Hone, *J. Chem. Soc. Chem. Commun.* **1993**, 778–779.
[29] F. Adar, in *The Porphyrins, Vol. 3* (Ed.: D. Dolphin), Academic Press, New York, **1979**, pp. 167–209.
[30] P. K. Warme, L. P. Hager, *Biochemistry* **1970**, *9*, 1606–1614.
[31] G. T. Babcock, W. R. Widger, W. A. Cramer, W. A. Oertling, J. G. Metz, *Biochemistry* **1985**, *24*, 3638–3645.
[32] a) D. Brault, M. Rougee, *Biochemistry* **1974**, *13*, 4591–4602; b) D. Brault, M. Rougee, *Biochem. Biophys. Res. Commun.* **1974**, *57*, 654–659.
[33] N. Greenfield, G. D. Fasman, *Biochemistry* **1969**, *8*, 4108–4116.
[34] a) R. Oekonomopoulos, G. Jung, *Biopolymers* **1980**, *19*, 203–214; b) T. S. Sudha, E. K. S. Yijayakumar, P. Balaram, *Int. J. Peptide Protein Res.* **1983**, *22*, 464–468; c) E. K. S. Yijayakumar, T. S. Sudha, P. Balaram, *Biopolymers* **1984**, *23*, 877–886; d) M. Mutter, K. H. Altmann, A. Florsheimer, J. Herbert, *Helv. Chim. Acta* **1986**, *69*, 786–792; e) M. C. Manning, R. W. Woody, *Biopolymers* **1991**, *31*, 569–586.
[35] S. Vuilleumier, M. Mutter, *Biopolymers* **1993**, *33*, 389–400.
[36] M. Nakano, H. Iwamaru, T. Tobita, *Biopolymers* **1982**, *21*, 805–815.
[37] a) F. D. Sonnichsen, J. E. Van Eyk, R. S. Hodges, B. D. Sykes, *Biochemistry* **1992**, *31*, 8790–8798; b) R. W. Storrs, D. Truckses, D. E. Wemmer, *Biopolymers* **1992**, 32, 1695–1702; c) A. Jasanoff, A. R. Fersht, *Biochemistry* **1994**, *33*, 2129–2135; d) A. Cammers-Goodwin, T. J. Allen, S. L. Oslick, K. F. McClure, J. H. Lee, D. S. Kemp, *J. Am. Chem. Soc.* **1996**, *118*, 3082–3090.
[38] a) Y. P. Myer, A. Pande, in *The Porphyrins, Vol. 4* (Ed.: D. Dolphin), Academic Press, New York, **1978**, pp. 271–321; b) Y. P. Myer, *Methods Enzymol.* **1978**, *54*, 249–284.
[39] M.-C. Hsu, R. W. Woody, *J. Am. Chem. Soc.* **1971**, *93*, 3515–3523.
[40] N. A. Nicola, E. Minasian, C. A. Appleby, S. J. Leach, *Biochemistry* **1975**, *14*, 5141–5149.
[41] a) Y. P. Myer, *J. Biol. Chem.* **1968**, *243*, 2115–2122; b) Y. P. Myer, *Biochemistry* **1968**, *7*, 765–776.
[42] P. A. Bullock, Y. P. Myer, *Biochemistry* **1978**, *17*, 3084–3091.
[43] a) E. E. Abola, F. C. Bernstein, S. H. Bryant, T. F. Koetzle, J. Weng, *Data Commission of the International Union of Crystallography*, F. H. Allen, G. Bergerhoff, R. Sievers, Bonn/Cambridge/Chester, **1987**, pp. 107–132; b) F. C. Bernstein, T. F. Koetzle, G. J. B. Williams, E. F. Meyer, Jr., M. D. Brice, J. R. Rodgers, O. Kennard, T. Shimanouchi, M. Tasumi, *J. Mol. Biol.* **1987**, *112*, 535–542.
[44] W. C. Johnson, Jr., *Methods Biochem. Anal.* **1985**, *31*, 61–163.

  0947-6539/97/0303-0349 $ 15.00+.25/0